Systematic Design of Virtual Component Method for Inverter-Based Microgrids

Po-Hsu Huang[1], Petr Vorobev[12], Mohamed Al Hosani[3], James L. Kirtley[1], and Konstantin Turitsyn[1]
[1]Massachusetts Institute of Technology
Cambridge, MA
[2]Skolkovo Institute of Science and Technology
Moscow, Russia
[3]Masdar Institute of Science and Technology
Abu Dhabi, UAE

***Abstract*—Control design of inverter-based microgrids plays a significant role in affecting dynamic performance of the system. Conventional microgrid droop control suffers from instability due to low X/R ratios and unique network characteristics as compared to large power systems. While many approaches such as virtual framework methods, virtual impedance methods, or synchronverters have been proposed and proven effective, an intuitive and fundamental insight into physical origins of instability has not yet been sufficiently disclosed. In this paper, a systematic approach for enhancing the stability of inverter-based microgrids is proposed. A test system is studied to derive simple and concise stability criteria based on the proposed Lyapunov function method. Particularly, we show that unlike in large-scale power systems, for microgrids the transient susceptance B' plays a crucial role in contracting the region of stable droop gains. Control schemes to minimize B' are then investigated, enabling a different perspective in views of the virtual component method. Finally, simulations are carried out to validate the proposed approach via direct time-domain analysis.**

***Index Terms*—Droop control, Lyapunov function, microgrids, small-signal stability.**

I. Introduction

Droop controlled inverter-based microgrids have gained a lot of attention recently in the development of future power networks due to the increasing penetration of distributed generation. In contrast to grid-connected modes, droop control islanding operations require more sophisticated control designs to ensure system stability [1]. Intense research works in recent years have provided comprehensive insights into the control and modeling of inverter-based microgrid systems [2]–[5]. Since the droop control concept originates from conventional power networks to achieve proper load sharing, the small-signal stability was first identified similar to the transmission level power grids. However, it was later realized that microgrid dynamics is noticeably different due to a much lower X/R ratio [6], [7]. That is, both the phase angle and voltage couple together and contribute to active and reactive power dependently. Therefore, the $P-\omega$ and $Q-V$ droop controls for low-voltage microgrids suffer from limited gain regions due to the deployment of highly resistive feeders to the point of coupling (PCC). Without the presence of additional coupling inductors, system stability is significantly compromised.

To address the coupling issues, the concept of virtual inductance has been proposed and widely appreciated due to its effectiveness [6], [8], [9]. The emulation of inductive dynamics helps to save bulky and costly inductors with enhancement of power sharing accuracy and stability. These methods, in general, introduce additional terms that reacts to the output currents into the reference voltages. Thus, the inverters act like an effectively controlled voltage source connected to their terminals through the virtual inductances. Also, the idea of synchronverters is earning a lot of attention as they are considered as grid friendly by mimicking the dynamics of synchronous machines [10]. Similar to the virtual inductance methods, slower rotor and stator dynamics are emulated by using high bandwidth two-loop controllers that regulate the current and voltage of output LC filters. All of these creative methods have been investigated and shown to be very effective. However, more intuitions and insights need to be carried out from a stability perspective.

This paper focuses on development of virtual components for enhancing the stability margin of inverter-based microgrids. Detailed explanations and clear intuitions are provided from a different viewpoint than the commonly used eigenvalue analysis. Although conducting eigenvalue extraction from a detailed model, in general, is not a computational burden for a small-scaled microgrid system, its numerical outcomes provide very limited information for understanding the system dynamics. Moreover, there exists distinction of participation of states into system modes, which have been reported in [11]. This leads to a more straight-forward representation of equations using a reduced-order model of high accuracy. Without loss of generality to a network setting, the problem is formulated using a simple two-bus system. Therefore, Lyapunov function candidates can be constructed to identify the important parameters that affect system stability. Based on the derived criteria, a new control design using the virtual component method is proposed to further improve the stability margin. Numerical simulation for a more complicated system

This work was supported by the Cooperative Agreement between the Masdar Institute of Science and Technology (Masdar Institute), Abu Dhabi, United Arab Emirates, and the Massachusetts Institute of Technology (MIT), Cambridge, MA, USA - Reference 02/MI/MI/CP/11/07633/GEN/G/00, The Ministry of Education and Science of Russian Federation, grant No. 14.615.21.0001, grant code: RFMEFI61514X0001, and NSF ECCS 1508666.

978-1-5386-2212-4/17/$31.00 ©2017 IEEE

is then carried out to verify the proposed method.

To sum up, key contributions of this paper are as follows: 1) detailed analysis of the system dynamical behaviors that provides insights into physical sources of instability; 2) derivation of simple and concise criteria to ensure system stability via the proposed Lyapunov function candidates; 3) development of the virtual component method for enhancing the stability region of the system.

II. Problem Formulation

In this paper, a commonly used comprehensive model with detailed control structure presented in [11] is employed. In general, the detailed model includes controller states of the voltage and current loops, resulting in higher system order. Although quasi-steady state approximation using time-scale separation may sometimes be a poor method as had been pointed out in [12], these fast controller modes do not directly participate into the slow droop modes. Therefore, by omitting the internal controller states, a simplified full model that enables the terminal voltage and frequency to be effectively controlled is obtained.

A. Two-Bus Model

To simplify the problem, a two-bus system is utilized for illustration. One can assume that the inverter is connected to a stiff bus (PCC) regulated by a group of inverters. Then, the ODEs of the system with three inverter and two current (aggregation of coupling and line inductances) states are given:

$$\dot{\theta} = \omega - \omega_0 \tag{1}$$

$$\tau\dot{\omega} = \omega_{ref} - \omega - k_p\omega_0 P \tag{2}$$

$$\tau\dot{V} = V_{ref} - V - k_q Q \tag{3}$$

$$L\dot{I}_d = V\cos\theta - V_s - RI_d + \omega_0 LI_q \tag{4}$$

$$L\dot{I}_q = V\sin\theta - RI_q - \omega_0 LI_d \tag{5}$$

where k_p and k_q are the $P-\omega$ and $Q-V$ droop gains in per-unit, respectively, V and V_s are the inverter and stiff bus voltages, respectively, and $\tau = w_c^{-1}$ is the time constant of the low-pass filter for the power measurement.

B. Reduced-Order Model

For large power systems, it is convenient to apply the quasi-steady state approximation, allowing one to treat (4) and (5) as algebraic equations by setting the derivative terms to zero. Consequently, the system order reduces to only three. However, for inverter-based microgrids this assumption is no longer valid as was shown in our recent work [12]. Particularly, the quasi steady-state assumption fails when the X/R ratio of the microgrid becomes comparable to unity. Therefore, a proper model order reduction technique has been proposed to account for the electromagnetic transients, which play a critical role in the onset of instability for microgrids [12]. To derive a reduced-order model, consider the dynamics of inductive line current being expressed in the following complex form:

$$I = I_d + jI_q = \frac{V\mathrm{e}^{j\theta} - V_s}{R + jX + sL} \tag{6}$$

where X is equal to $\omega_0 L$ and ω_0 indicates the nominal frequency. Applying the Taylor series expansion on the Laplace operator s, the line current can be approximated by neglecting the high-order terms:

$$I \approx I^0 - \frac{L}{R+jX} sI^0. \tag{7}$$

where $I^0 = (R+jX)^{-1}\left(V\mathrm{e}^{j\theta} - V_s\right)$ and supersrcipt $\{0\}$ denotes the zero-order term. Therefore, active and reactive power can be expressed as:

$$P = \mathfrak{Re}[VI^*] \approx P^0 - G'V\dot{V} - B'V^2\dot{\theta} \tag{8}$$

$$Q = \mathfrak{Im}[VI^*] \approx Q^0 - B'V\dot{V} + G'V^2\dot{\theta}, \tag{9}$$

where

$$P^0 = BVV_s\sin\theta + G(V^2 - VV_s\cos\theta), \tag{10}$$

$$Q^0 = B(V^2 - VV_s\cos\theta) - GVV_s\sin\theta, \tag{11}$$

$$G = R/(R^2+X^2),\ B = X/(R^2+X^2) \tag{12}$$

$$G' = \frac{L(R^2-X^2)}{(R^2+X^2)^2},\ B' = \frac{2LXR}{(R^2+X^2)^2}. \tag{13}$$

and G' and B' stand for the transient conductance and susceptance. Substituting (8) and (9) into eqs. (1)-(3), the linearized model at the nominal operating point can be obtained:

$$\lambda_p\tau\ddot{\theta} + (\lambda_p - B')\,\dot{\theta} + B\theta + G\upsilon - G'\dot{\upsilon} = 0 \tag{14a}$$

$$(\lambda_q\tau - B')\,\dot{\upsilon} + (\lambda_q + B)\upsilon - G\theta + G'\dot{\theta} = 0 \tag{14b}$$

where $\lambda_p = (k_p\omega_0)^{-1}$ and $\lambda_q = k_q^{-1}$. For simpler expressions, we abuse the notation of defining $\theta = \delta\theta$ and $\upsilon = \delta V$. Also, the assumption is made that the operating points are close to the nominal condition as $\theta \approx 0$, and $V_s = V = V_n \approx 1\ pu$, which is valid as the capability of the lines in microgrids is normally greater than the rating of the inverters.

III. Stability Assessment

From (14a) and (14b), it can be observed that the quasi-steady-state approximation is the results of setting G' and B' to zeros. However, these two terms have significant impacts on predicting instability. A simple observation can be made on the second term (damping) of (14a) that λ_p being less than B' contributes to instability due to negative damping. To be more legitimate, the global stability of a linear system could always be certified by ensuring that the real parts of all eigenvalues are strictly less than zero. While the solution exists for such a simple system, their cumbersome expressions may divert the analysis to numerical trials without much intuition.

A more qualitative way of obtaining stability certificate is to search for Lyapunov function candidates. That is, one can certify the stability of a linear system $\dot{\mathbf{x}} = \mathbf{A}\mathbf{x}$ by finding a Lyapunov function, $W(\mathbf{x}) > 0$ for $\mathbf{x} \neq \mathbf{0}$, being strictly

978-1-5386-2212-4/17/$31.00 ©2017 IEEE

decaying with respect to time, $dW(\mathbf{x})/dt < 0$. First, eq. (14a) by is multiplied by $2\tau\dot{\theta} + \theta$ to obtain:

$$\begin{aligned} &\frac{d}{dt}\left\{\frac{\lambda_p(\tau\dot{\theta}+\theta)^2}{2} + \frac{(2\tau B - B')\theta^2}{2} + \frac{\tau^2\lambda_p\dot{\theta}^2}{2}\right\} \\ &+ \tau(\lambda_p - 2B')\dot{\theta}^2 + B\theta^2 + G\theta\upsilon - G'\theta\dot{\upsilon} \\ &+ 2\tau G\dot{\theta}\upsilon - 2\tau G'\dot{\theta}\dot{\upsilon} = 0. \end{aligned} \tag{15}$$

Similarly, multiplying eq. (14b) by $2\tau\dot{\upsilon} + \upsilon$ gives:

$$\begin{aligned} &\frac{d}{dt}\left\{\frac{(3\tau\lambda_q + 2\tau B - B')\upsilon^2}{2} + (2\tau G + G')\theta\upsilon\right\} \\ &+ (\lambda_q + B)\upsilon^2 + 2(\tau^2\lambda_q + \tau B')\dot{\upsilon}^2 - G\theta\upsilon \\ &- G'\theta\upsilon - 2\tau G\dot{\theta}\upsilon - 4\tau G\theta\dot{\upsilon} + 2\tau G'\dot{\theta}\dot{\upsilon} = 0. \end{aligned} \tag{16}$$

Therefore, the terms inside the curly brackets after the summation of (15) and (16) form a Lyapunov function $W(\mathbf{x}) = \frac{1}{2}\mathbf{x}^T\mathbf{P}\mathbf{x}$, where $\mathbf{x} = [\tau\dot{\theta} + \theta, \dot{\theta}, \theta, \upsilon]^T$ and

$$\mathbf{P} = \begin{bmatrix} \lambda_p & 0 & 0 & 0 \\ 0 & \tau^2\lambda_p & 0 & 0 \\ 0 & 0 & 2\tau B - B' & 2\tau G + G' \\ 0 & 0 & 2\tau G + G' & 3\tau\lambda_q + 2\tau B - B' \end{bmatrix}. \tag{17}$$

Whenever $\omega_0\tau \gg X/R$ and $X/R \neq 0$, it is safe to assume that $G' \ll \tau G$ and $B' \ll \tau B$. Therefore, the criteria for $\mathbf{P}$ being positive definite simplify to:

$$\lambda_p > 0 \tag{18a}$$

$$(3\tau\lambda_q + 2\tau B) - (2\tau G)(2\tau B)^{-1}(2\tau G) > 0 \tag{18b}$$

For the decay rate, one can then derive $\dot{W(\mathbf{x})} = -\mathbf{y}^T\mathbf{Q}\mathbf{y}$, where $\mathbf{y} = [\tau\dot{\theta}, \theta, \tau\dot{\upsilon}, \upsilon]^T$ and

$$\mathbf{Q} = \begin{bmatrix} \frac{\lambda_p - 2B'}{\tau} & 0 & 0 & 0 \\ 0 & B & -2G - \frac{G'}{\tau} & 0 \\ 0 & -2G - \frac{G'}{\tau} & 2\lambda_q - \frac{2B'}{\tau} & 0 \\ 0 & 0 & 0 & \lambda_q + B \end{bmatrix}. \tag{19}$$

The criteria for $\mathbf{Q}$ becomes:

$$\lambda_p > 2B' \tag{20a}$$

$$(2\lambda_q - 2B'/\tau) - (2G)B^{-1}(2G) > 0 \tag{20b}$$

In fact, eq. (18a) can be always satisfied and (20b) is stricter than (18b). Therefore, the stability certificate via the proposed Lyapunov function can be ensured by the following conditions:

$$k_p < \frac{1}{2\omega_0 B'} \tag{21a}$$

$$k_q < \frac{\tau B}{2\tau G^2 + BB'} \tag{21b}$$

The obtained conditions are sufficient (although conservative) for stability of the system. They also illustrate the effect of B' on the system stability. Particularly, the active power-frequency mode suffers significantly from the increase of B' (analogy to transient susceptance). Fig. 1 shows the comparison between the exact and predicted stability regions with the prediction on k_p being approximately 50% conservative

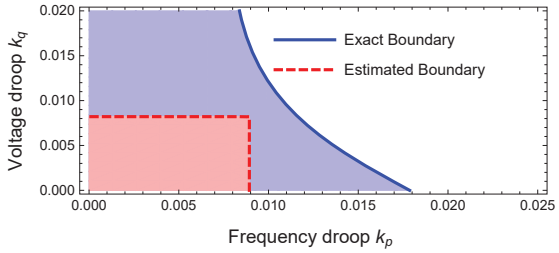

Fig. 1. Stability regions of the system ($X = 0.008\ pu$, $R = 0.009\ pu$)

(which is acceptable piratically since one always operate with substantial stability margin) when k_q is sufficiently small. In order to certify a wider range of stability, one can parametrize the multiplier terms, $c\tau\dot{\theta} + \theta$ and $c\tau\dot{\upsilon} + \upsilon$. The search of such an extended class of Lyapunov functions is the subject of subsequent work.

IV. Emulation of Virtual Components

In the previous section, it was shown that B' deteriorates the damping coefficient, which results in limiting the stability regions of the droop-controlled inverter system. This transient susceptance normally increases when the coupling between the inverter and PCC becomes stronger (decrease of impedance). It has been reported in [8] that additional coupling inductor should be placed to enhance the satbility performance; thus the implementation of additional coupling inductors can be commonly seen. However, placement of bulky inductors is not always a desirable solution, so many research works have proposed the concept of virtual impedances, virtual inductances or virtual synchronous generators that mimic the stator windings and rotor dynamics [6], [8]–[10]. All these methods help to mitigate the system instability, which will be investigated in this section.

A. Virtual Inductance

The typical inverter control system utilizes a two-loop control scheme where the feed-forward terms with the inner current loop are designed to achieve higher bandwidth than the outer voltage loop such that the controller parameters can be tuned independently. In general, the overall time constant of the voltage regulation is far smaller than that of the droop mode. Therefore, one can consider a fast regulation of the inverter terminal voltage and neglect the LC filters. To mimic the virtual impedance (or equivalently generators' stator windings), additional terms that react to the output currents are added to emulate the inductive dynamics. That is, the modified reference voltages are of the following forms:

$$V_d^{ref} = \bar{V}_d^{ref} + X_m I_{oq} - \frac{s\omega_f L_m}{s + \omega_f} I_{od} \tag{22a}$$

$$V_q^{ref} = \bar{V}_q^{ref} - X_m I_{od} - \frac{s\omega_f L_m}{s + \omega_f} I_{od} \tag{22b}$$

where $X_m = \omega_0 L_m$ denotes the virtual reactance, ω_f is the cut-off frequency of the high-pass filter, $\bar{V}_{d,q}^{ref}$ correspond to the dq voltage commands from the reactive power droop

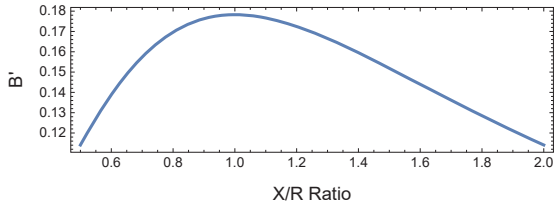

Fig. 2. Variation of B' with respect to X/R ratio

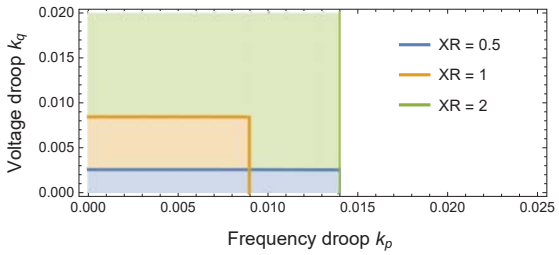

Fig. 3. Predicted stability regions for different X/R ratios

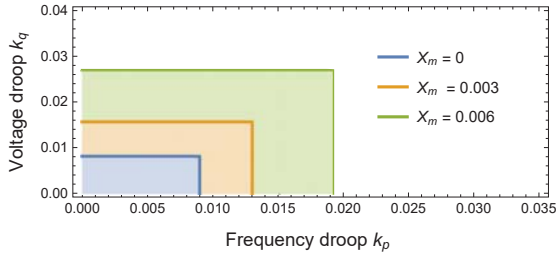

Fig. 4. Predicted stability regions for different X_m in per-unit

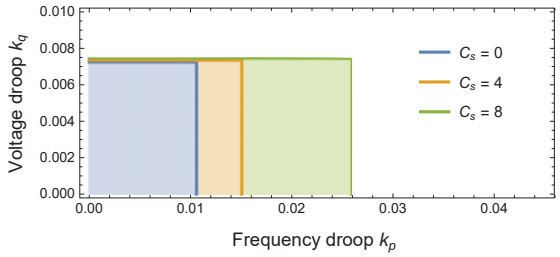

Fig. 5. Predicted stability regions for different C_s ($R_s = 0.0024\ pu$)

(normally with $\bar{V}_q^{ref}$ set to zero), $V_{d,q}^{ref}$ are the modified reference voltage for the two-loop control scheme, and $I_{od,oq}$ are the output currents in $d-q$ axis. One can note that the above mentioned control scheme may have different equivalent forms that result in the same dynamic behavior, and here we follow a similar configuration as proposed in [6]. In addition, the effectiveness of the emulation is subject to the closed-loop stability and controller bandwidth; hence, proper parameter tuning of the two-loop controller is required but not disclosed in this paper. With the deployment of the virtual inductance, expansion of the stability region can be explained by considering the change of $B' = \frac{2RX^2}{\omega_0 Z^4}$, whose variation with X/R ratio is shown in Fig. 2, where $X = \omega_0(L_m + L_t)$ and $R = R_t$. Here L_t and R_t are the aggregated coupling and line inductance and resistance, respectively. It can be seen that the maximum of B' occurs at $X/R = 1$, implying that bidirectional perturbation of X/R away from unity allows expansion in stability range of k_p provided that k_q is sufficiently small. However, decreasing X/R may further lead to shrinking the stability region, which can be seen in Fig. 3. In general, it is more beneficial to properly select the virtual inductance to ensure $X/R > 1$ for further expansion of stability region.

B. Virtual Reactance

The advantages of adding a virtual inductance into the control scheme have been identified in the previous subsection.. Another approach is to add only reactance X_m without its dynamic part. In this case, we can simply set L_m in eqs. (22a) and (22b) to zero. Let's consider now the original expression of B' in (13) as $\frac{2XRL}{Z^4}$ with an intentional separation of L and X implying that they can be manipulated independently. In fact, increasing X while setting L_m to zero can further reduce B'. Note that we implicitly define $X = X_m + X_t$, $R = R_t$ and $L = L_t$. The resulting stability regions are shown in Fig. 4, indicating that there is no clear benefits of increasing L_m in stabilizing the droop modes. In fact, L_m increases B' and further limits the stability regions. This interesting finding suggests that one can tune L_m and X_m separately for the virtual component methods to strengthen the system stability.

C. Virtual Capacitance

It has been demonstrated that B' can be manipulated by changing X and L independently. Although the increase of X can significantly benefit the system stability, it may reduce the voltage regulation accuracy. In fact, one may also think about canceling the effect of inductance L_t without increasing the overall reactance $X = X_m + X_t$. Here, we propose a simple method to use the low-pass filters instead of the high-pass ones, which mimic a dynamic capacitance C_s in parallel with a resistance R_s, into reference voltages:

$$V_d^{ref} = \bar{V}_d^{ref} - \frac{1/C_s}{s + 1/(R_s C_s)} I_{od} \tag{23a}$$

$$V_q^{ref} = \bar{V}_q^{ref} - \frac{1/C_s}{s + 1/(R_s C_s)} I_{oq} \tag{23b}$$

By choosing sufficiently large values of $1/(R_s C_s)$, the equation correlating voltage and current can be linearized as:

$$\delta V \approx R_s \delta I - R_s^2 C_s \dot{\delta I} \tag{24}$$

Eq. (24) shows that the terminal voltage reacts negatively to the derivative of current, which behaves like a negative inductance. Therefore the effective B' reduces, leading to expansions of stability regions as shown in Fig. 5.

V. Numerical Verification

In this section, simulation results are carried out to verify the proposed control methods. A system with three inverters in a cascade configuration is built based on the full model described in eqs. (1)-(5) (including the state variables of all

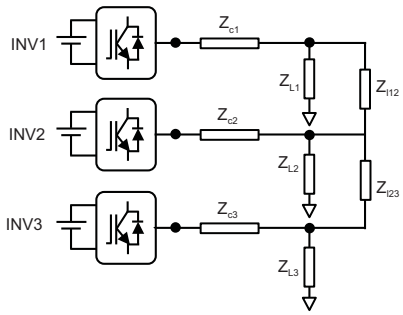

Fig. 6. Three inverter microgrid configuration

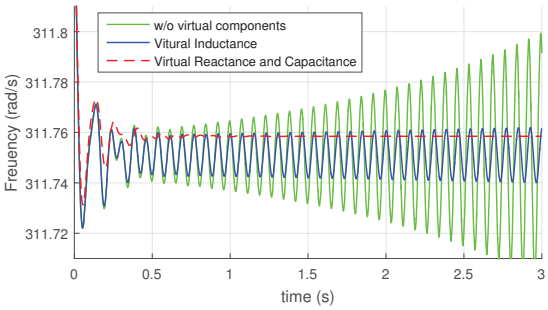

Fig. 7. Time-domain results ($k_p = 0.9\%$, $k_q = 1\%$)

line/coupling inductances), as shown in Fig. 6. The system parameters are: base peak phase voltage: $381.58\,\mathrm{V}$; base inverter rating: $10\,\mathrm{kVA}$; nominal frequency: $2\pi{\times}50\ \mathrm{rad/s}$; coupling impedance: $0.03 + 0.11i\Omega$; line inductance: $0.26\,\mathrm{mH\,km^{-1}}$; line resistance: $165\,\mathrm{m\Omega\,km^{-1}}$; line length: $[3,\ 2]\,\mathrm{km}$; bus load: $[25 + 4.7i,\ 20 + 3.77i,\ 22 + 3.14i]\ \Omega$.

The time-domain simulation is conducted to compare the dynamic responses between the different methods, shown in Fig. 7. For the virtual capacitance method, the cut-off frequency of the filter is set to be $1/(R_sC_s) = 100\ \mathrm{rad/s}$ to capture the unstable modes, and the equivalent negative inductance $R_s^2C_s$ is selected to cancel a fraction of the coupling inductance. Therefore, the overall virtual parameters in per-unit are chosen with L_m being $3e^{-4}/\omega_0\ pu$ and R_s and C_s being $1.4e{-}3\ pu$ and $7.207\ pu$, respectively. The result shows that the virtual components play a significant role in stabilizing the system. A more aggressive case is then demonstrated in Fig. 8 with higher droop gains of $k_p = 2\%$, $k_q = 2\%$ and a higher virtual inductance of $L_m = 0.006/\omega_0\ pu$. It can be seen that the addition of virtual reactance and/or capacitance method tends to enhance the system stability, verifying the effectiveness of the proposed approach.

VI. Conclusion

Proper control design for droop-based inverters is crucial for enhancement of dynamic performance. Particularly, the transient suscepntacne B' deteriorates the damping coefficient of the embedded phase angle oscillator. Based on the proposed Lyapunov method, the effect of B' on the system instability

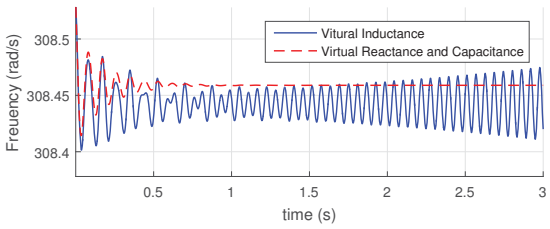

Fig. 8. Time-domain results ($k_p = 2\%$, $k_q = 2\%$)

was illustrated, and methods for enhancing the system stability are proposed consisting of emulating the proper virtual impedance components. The results suggest that the increase of only the reactance X_m can achieve a wider stability region as compared to the conventional methods. Moreover, cancellation of inductive dynamics, which is shown to be largely responsible for the onset of instability, is further exploited with the proposed virtual capacitance method. The effectiveness of the proposed approaches is justified by theoretical analysis and confirmed by direct time-domain simulation based on the full model. A possible extension of the method to provide a better stability assessment is discussed which is the subject of subsequent work together with the generalization to arbitrary network configuration.

References

[1] N. Hatziargyriou, H. Asano, R. Iravani, and C. Marnay, "Microgrids," *IEEE Power Energy Mag.*, vol. 5, no. 4, pp. 78–94, 2007.

[2] D. E. Olivares, A. Mehrizi-Sani, A. H. Etemadi, C. A. Canizares, R. Iravani, M. Kazerani, A. H. Hajimiragha, O. Gomis-Bellmunt, M. Saeedifard, R. Palma-Behnke *et al.*, "Trends in microgrid control," *IEEE Trans. Smart Grid*, vol. 5, no. 4, pp. 1905–1919, 2014.

[3] S. Parhizi, H. Lotfi, A. Khodaei, and S. Bahramirad, "State of the art in research on microgrids: a review," *Access, IEEE*, vol. 3, pp. 890–925, 2015.

[4] Y. Han, H. Li, P. Shen, E. Coelho, and J. Guerrero, "Review of active and reactive power sharing strategies in hierarchical controlled microgrids," *IEEE Trans. Power Electron., in press*, 2016.

[5] A. Tuladhar, H. Jin, T. Unger, and K. Mauch, "Control of parallel inverters in distributed ac power systems with consideration of line impedance effect," *IEEE Trans. Ind. Appl.*, vol. 36, no. 1, pp. 131–138, Jan 2000.

[6] J. M. Guerrero, L. G. de Vicuna, J. Matas, M. Castilla, and J. Miret, "Output impedance design of parallel-connected ups inverters with wireless load-sharing control," *IEEE Trans. Ind. Electron.*, vol. 52, no. 4, pp. 1126–1135, Aug 2005.

[7] N. Hatziargyriou, *Microgrids: architectures and control*. John Wiley & Sons, 2013.

[8] J. He and Y. W. Li, "Analysis, design, and implementation of virtual impedance for power electronics interfaced distributed generation," *IEEE Trans. Ind. Appl.*, vol. 47, no. 6, pp. 2525–2538, Nov 2011.

[9] J. He, Y. W. Li, J. M. Guerrero, F. Blaabjerg, and J. C. Vasquez, "An islanding microgrid power sharing approach using enhanced virtual impedance control scheme," *IEEE Trans. Power Electron.*, vol. 28, no. 11, pp. 5272–5282, Nov 2013.

[10] Q. C. Zhong and G. Weiss, "Synchronverters: Inverters that mimic synchronous generators," *IEEE Trans. Ind. Electron.*, vol. 58, no. 4, pp. 1259–1267, April 2011.

[11] N. Pogaku, M. Prodanović, and T. C. Green, "Modeling, analysis and testing of autonomous operation of an inverter-based microgrid," *IEEE Trans. Power Electron.*, vol. 22, no. 2, pp. 613–625, 2007.

[12] P. Vorobev, P.-H. Huang, M. A. Hosani, J. L. Kirtley, and K. Turitsyn, "High-fidelity model order reduction for microgrids stability assessment," arXiv:1611.01761[cs.SY].

978-1-5386-2212-4/17/$31.00 ©2017 IEEE